Journal of Building Engineering 96 (2024) 110535

Contents lists available at ScienceDirect

Journal of Building Engineering

journal homepage: www.elsevier.com/locate/jobe

Effect of ZnAl-NO_2 LDH on chloride entrapment and protection of iron reinforcement in mortar samples

R.S. Sampaio *, C. Gomes, A.C. Bastos, M.G.S. Ferreira

DEMaC – Department of Materials and Ceramic Engineering, and CICECO – Aveiro Institute of Materials, Universidade de Aveiro, 3810-193, Aveiro, Portugal

ARTICLE INFO

Keywords:
LDH
Layered double hydroxides
ZnAl-NO_2
Chloride
Corrosion

ABSTRACT

Layered double hydroxides (LDHs) have gained attention in the concrete research field, appearing as prospective additives for controlling chloride attack, and as micro or nano deliverers of corrosion inhibitors. This work reports the effect of ZnAl-NO_2 LDH on the evolution of chloride concentration in the pore solution and on the corrosion resistance of iron in mortar samples exposed to 3.5 % NaCl solution. To this end, Ag/AgCl sensors were used to monitor the ingress of chloride ions into mortar, while the electrochemical state of the iron was evaluated by electrochemical impedance spectroscopy. Furthermore, the mortars were analyzed by XRD and TGA, and the total amount of chloride was measured with a commercial sensor. Mortars with LDH showed a slower increase of chloride ions in the pore solution and the preservation of the passive state of the Fe. The presence of LDHs did not cause a significant structural change in the mortars, which was evidenced by the similar distribution of the high frequency resistance as a function of depth in the samples with and without the additive. Finally, the amount of bound chloride in the cementitious material was higher in the LDH-containing mortars. In conclusion, ZnAl-NO_2 LDH exhibited a positive effect on the protection of reinforcement embedded in mortar samples when subjected to chloride ingress.

1. Introduction

Exposure to marine conditions represents a major problem in the durability of reinforced concrete structures [1]. The presence of a certain amount of chloride ions in the interfacial pore solution to the surface of the steel reinforcement leads to a localized breakdown of its protective film, which is spontaneously formed due to the alkaline nature of cementitious materials [1]. The chloride content necessary to initiate the localized attack on the passive layer of steel is known as the critical chloride content or chloride threshold value. The service life of concrete structures exposed to marine environment can be divided in two different stages, as proposed by Tuuti's corrosion model [2]. The initiation stage is related to the increase in the chloride content at the reinforcement level until the critical value is reached. The propagation phase is related to the evolution of the corrosion stage and the consequent degradation of the concrete cover. The variation of the chloride content in the pore solution depends on the ease of penetration of chloride ions through the concrete cover and the ability of concrete to bind chlorides. The penetration of chlorides into the concrete matrix occurs by diffusion, capillary suction, and permeation, and, therefore, chloride ingress is mainly affected by the pore structure of concrete and exposure conditions. The main factors that affect concrete porosity are water/cement ratio, concrete composition and curing

* Corresponding author.
E-mail address: ruimssampaio@tecnico.ulisboa.pt (R.S. Sampaio).

https://doi.org/10.1016/j.jobe.2024.110535
Received 19 June 2024; Received in revised form 10 August 2024; Accepted 20 August 2024
Available online 22 August 2024

conditions (temperature and aging/degree of hydration). The chloride content in the pore solution is also affected by the ability of concrete to partly immobilize chlorides. The hydration products of cement can react with chlorides leading to the formation of calcium chloroaluminates, like Friedel's salt for example [3]. However, a decrease in the pH of the pore solution can lead to the dissolution of the chloroaluminates and consequent release of bound chlorides into solution [4].

The protection of reinforced concrete structures can be carried out by acting specifically on the different elements that make up these structures (cementitious layer and reinforcing steel bar). In the case of the reinforcement, it can be coated by a zinc film (galvanization) or an epoxy layer, cathodically protected, or substituted by a less active material, such as stainless steel. In the case of the cementitious material, the layer of concrete between the environment and the rebar can be thicker, less porous, coated with paint, and mixed with corrosion inhibitors or additives with the ability to capture chlorides. The addition of a corrosion inhibitor has some advantages, namely the lower cost and simplicity.

Layered double hydroxides (LDHs) have been recently studied as additives in concrete composition for corrosion inhibitor release and aggressive anions capture [5–7]. LDHs are layered compounds having the following chemical formula: $\left[M_{1-x}^{2+}M_x^{3+}(OH)_2\right]A_{x/n}^{n-}.yH_2O$, where M^{2+} and M^{3+} are divalent and trivalent metal cations, respectively, A^{n-} is an interlayer anion, and x is the $M^{3+}/(M^{2+}+M^{3+})$ molar ratio. The interlayer anions can be easily exchanged with other anions of higher affinity. For many LDH, the order of exchange affinity has been found to be: $NO_3^- < NO_2^- < Cl^- < OH^- < SO_4^{2-} < CO_3^{2-}$ [8].

The effect of LDH on chloride entrapment and corrosion inhibitor release in cementitious environment has been investigated. Several LDHs demonstrated the ability to capture chlorides. Mg-Al LDH were tested in simulated concrete pore solution and promoted a corrosion inhibition effect on a steel electrode due to chlorides uptake by anionic exchange, and to inhibitor release (NO_3^-) [9,10]. The addition of Ca-Al LDHs to mortar samples led to the decrease of chloride migration coefficient due to the increase of mortar tortuosity and chloride capture ability [11]. However, only a few studies were performed in hardened samples [11–14] and none used embedded sensors for chloride detection. Despite being one of the least studied LDHs [7,15], Zn-Al LDH has already demonstrated the ability to capture chlorides and consequently improve corrosion resistance of a substrate when applied in coatings [16–18]. In cementitious environmment it was only tested in simulated pore solution [5,6]. Zn-Al LDH exhibited higher chloride binding capacity comparing to Mg-Al LDH and Ca-Al LDH due to its greater basal spacing [5]. Although this LDH has great potential for application in cementitious structures, no study with this additive in hardened samples has yet been reported. As such, this work fills a gap in scientific knowledge regarding the action of this specific type of LDH on chloride entrapment in hardened mortar samples.

The evaluation of the effect of LDHs on chloride capture in cementitious samples can be carried out by several methods, which can be divided into destructive and non-destructive. The most used destructive methods are the leaching technique and pore solution expression method, which require the extraction of a representative sample from the structure under study. However, the heterogeneity of concrete and the sample preparation procedure leads to significant measurement errors [19,20]. The non-destructive methods are mainly divided in embedded sensors [21], and electromagnetic techniques, which allow external contactless measurement [19,22]. These electromagnetic techniques require heavy and expensive equipment, and therefore, they are sometimes used in a destructive approach through the analysis in laboratory of a sample taken from the in-service structure.

The monitoring of chlorides using embedded sensors, is non-destructive and permits a more reliable *in-situ* assessment since it is only sensitive to the chloride ions present in the pore solution. Commercial potentiometric sensors exist in the market for chemical analysis of chloride. However, they are not suitable for embedding in mortar because they are fragile. They are also too large to be useful for the characterization planed in this work. For this purpose, a thin wire presents a more adequate geometry for an accurate measurement without being invasive to the cementitious structures [23,24].

For chloride sensing, among several materials that have been studied (such as some doped conducting polymers [25,26]), silver/silver chloride sensors are the most reliable due to their higher sensitivity and response time compared to other materials [27]. The high reversibility of the Ag/Ag^+ couple in chloride environments provides a useful application of these electrodes. The equilibrium that is established at the Ag/AgCl interface can be written as [28]:

$$Ag + Cl^- \leftrightarrow AgCl + e^- \tag{1}$$

and the equilibrium potential is given by the Nernst equation:

$$E = E^0 - 2.3\frac{RT}{nF}\log a_{Cl^-} \tag{2}$$

where E^0 is the standard equilibrium potential, R is the universal constant of ideal gas, T is the temperature, n is the number of electrons involved in the reaction, F is the Faraday constant and a_{Cl^-} is the activity of the chloride ion (often replaced by concentration in the calibration step). Since the equilibrium is established at the silver/silver chloride interface it is important that the silver chloride coat be porous and thin enough to allow a faster penetration (diffusion) of chloride ions into the interface and to improve the response time, respectively [29,30].

The synthesis of Ag/AgCl electrodes can be done by different electrochemical or thermal methods: anodization of a silver substrate [31]; cathodic electrodeposition of silver on a conducting substrate (stainless steel, glassy carbon, etc.) followed by anodic deposition of silver chloride [32]; thermal decomposition in a furnace of a paste of silver oxide, silver chlorate, and water to form the couple Ag/AgCl [33]; and thermal reduction of silver oxide paste followed by electrolytic formation of the silver chloride [32].

The main objective of this work was to characterize *in situ* the effect of LDH-NO_2 on the entrapment of chlorides and on the corrosion of iron electrodes embedded in mortar samples. For that, combs (Fig. 1) with 8 chloride sensors made of electrochemically synthetized Ag/AgCl were embedded in mortar samples, with and without LDH, to monitor the evolution of chloride content in the

pore solution as a function of depth. Combs with Fe electrodes were prepared and exposed in a similar way to monitor the corrosion as a function of depth and the effect of the LDH-NO_3 and LDH-NO_2 as additives to the mortar. The experiments were complemented by X-ray diffraction (XRD) and thermogravimetric analysis (TGA) performed on samples taken from different depths of mortars immersed for different periods.

2. Experimental procedure

2.1. Materials

For preparing the chloride sensors, 1.5 cm segments of 0.8 mm diameter silver wire (99.99 % pure, Goodfellow, UK) were connected to an electrical cable with colloidal silver suspension (Ted Pella Inc, USA), and the connection reinforced and isolated with epoxy resin (Araldite) – Fig. 1 a). The electrodes were polished before connection with SiC paper up to grit 4000 and cleaned with acetone and Millipore water to remove contaminations. The synthesis and characterization of the sensors is described in section 3.1. For corrosion testing, 1.5 cm segments of 1 mm diameter iron wire (99.90 % pure, Goodfellow, UK) were prepared in the same way as detailed above. All Ag or Fe electrodes were isolated with Lacomit varnish (Agar Scientific, UK) to a final active surface length of about 5 mm – Fig. 1 a). The ZnAl-NO_3 and ZnAl-NO_2 LDHs used in this work were produced by Smallmateck (Aveiro, Portugal) using the co-precipitation method. The synthesis was made by slow addition of 0.5 M $Zn(NO_3)_2{\cdot}6H_2O$ and 0.25 M $Al(NO_3)_3{\cdot}9H_2O$ to 1.5 M $NaNO_3$ (for ZnAl-NO_3) or $NaNO_2$ (for ZnAl-NO_2), while keeping the pH = 10 by the addition of 2 M NaOH. More details about the synthesis and characterization of the LDH can be found in Refs. [6,34].

2.2. Electrodes assembly

The chloride sensors and the iron wires were grouped in 8-electrode combs with a spacing of 5 mm between each wire – Fig. 1 b). The assembly of the chloride sensors was carried out after silver anodizing and potentiometric characterization of each modified electrode. Afterwards, the combs were embedded perpendicular to the surface in the centre of mortar samples with 5 × 5 cm^2 base area and 6.5 cm height. The top sensor was positioned 5 mm below the mortar top surface. For this purpose, maritime plywood moulds were used for the hardening of the mortar samples allowing the passage of the electrical cables and keeping the combs perpendicular to the top face at the desired distance. The mortar composition is presented in Table 1. It was chosen for obtaining a sufficiently porous cementitious matrix to accelerate the penetration of the aggressive agents. Reference mortars (without LDH) and mortars with LDH-NO_3 and LDH-NO_2 were prepared with either chloride sensors or with iron electrodes for corrosion measurements. Samples for XRD and TGA analysis were produced without electrodes. The mortars hardened inside the moulds for 1 week after which they cured for 2 weeks immersed in distilled water. Finally, all the faces of the mortar samples were isolated with Araldite epoxy resin with exception of the top face (perpendicular to the set of sensors), as shown in Fig. 1 c).

2.3. Chloride monitoring

The chloride content inside the mortars was determined by measuring the open circuit potential of each sensor versus a saturated calomel electrode (SCE), as shown in Figs. 1 c) and Fig. 2. The potential difference was converted to chloride concentration by applying calibration curves obtained for each individual sensor prior to the embedment. The mortars were immersed in aqueous 3.5 % NaCl

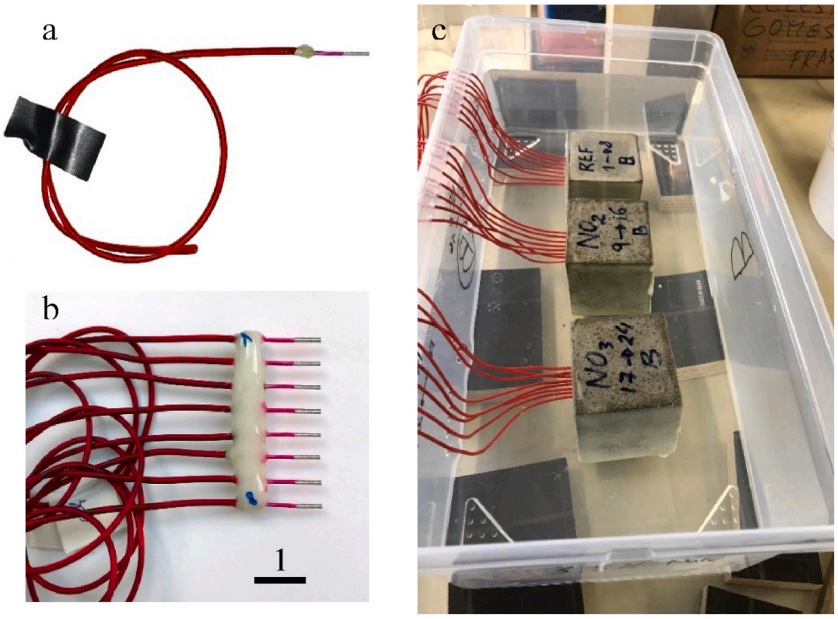

Fig. 1. a) Silver electrode before anodizing, b) comb with assembly of 8 electrodes, c) mortar samples with embedded electrodes immersed in aqueous 3.5 % NaCl.

Table 1
Mortar composition.

Mortar composition	Mass %
Cement I 42.5N	20.83
LDH (<125 μm)	0 or 2
Sand 0–2 mm	62.50
Water	16.67
Water/Cement ratio	0.8
Sand/Cement ratio	3

solution to simulate the sea conditions and the measurements started immediately after immersion. The measuring equipment was a CompactStat potentiostat coupled to a peripheral differential amplifier (PDA) (input impedance of 10^{12} Ω) both from Ivium Technologies (The Netherlands).

2.4. Corrosion testing

The corrosion of Fe wires embedded at different depths in the mortars was monitored by open circuit potential (OCP) and by electrochemical impedance spectroscopy (EIS). The OCP was measured as described in section 2.3. The EIS measurements were performed using the CompactStat potentiostat in a three-electrode arrangement, with the embedded iron wires as working electrodes, a SCE as reference, and a platinum counter electrode, immersed in the 3.5 % NaCl solution. The spectra were acquired at OCP with a sine wave perturbation of 10 mV rms in the frequency range from 100 kHz to 1 mHz with 10 points per decade with logarithmic distribution.

2.5. Mortar characterization

After different immersion times, the central cores of reference mortars and LDH-containing mortars were dry cut and transversely sliced into 5 mm pieces. Each fragment was ground with an agate mortar and pestle. The powders were analyzed by x-ray diffraction (XRD) with a Panalytical X'Pert PRO3 diffractometer (Almelo, Netherlands), between 2θ Bragg angles of 5° and 25° using a step size of 0.02°. Thermogravimetric analysis (TGA) was performed with a Hitachi STA7200 using about 10 mg of powder in an alumina crucible. The weight loss of the samples was determined in a heating temperature range from 30 to 800 °C at a rate of 10 °C/min and purging

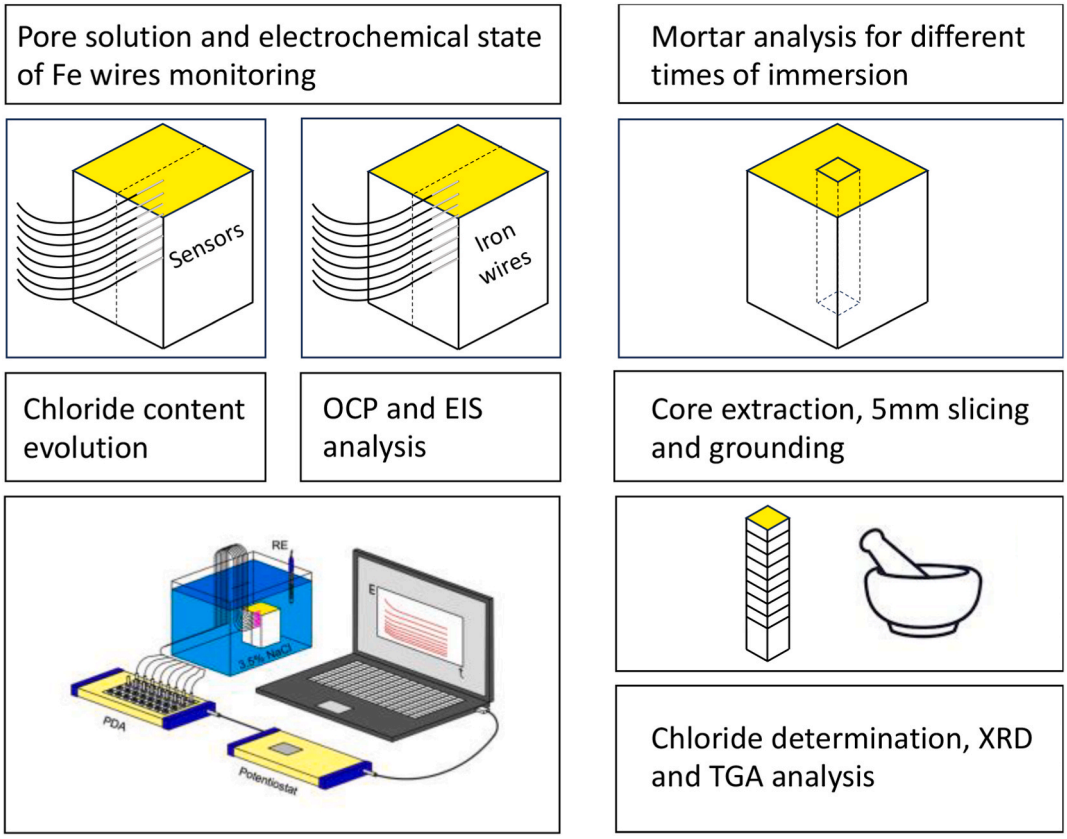

Fig. 2. Illustration of the overall experiment.

with 200 mL/min of nitrogen. The chloride content was determined using a commercial chloride ion-selective sensor (Mettler Toledo). For this, 0.4 g of each powder was added to 16 mL of Millipore water and ultrasonicated for 2 min. The surface of the modified electrodes was observed by scanning electron microscopy using a Hitachi SU-70 microscope.

3. Results and discussion

3.1. Synthesis and characterization of sensors

The synthesis of Ag/AgCl films was performed galvanostatically with a pulse of 2 mA cm^{-2} for 30 min in a 0.1 M HCl solution. The

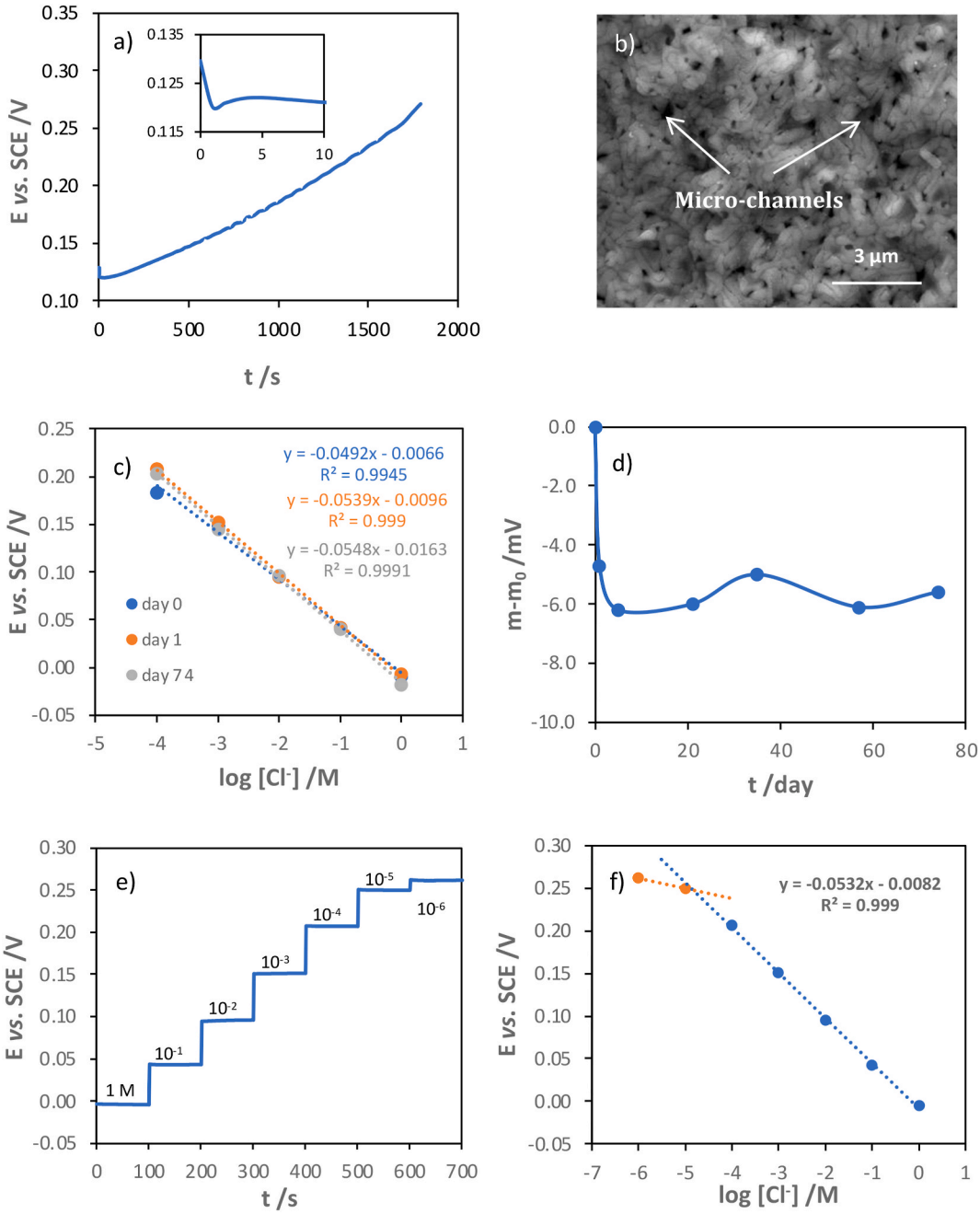

Fig. 3. E-t transient of Ag/AgCl synthesis at 2 mA cm^{-2} for 30 min in 0.1 M HCl aqueous solution (a), SEM image of the surface of the Ag/AgCl electrode (b), evolution of the calibration curve of Ag/AgCl sensor immersed in saturated $Ca(OH)_2$ solution for 74 days (c), variation of curve calibration slope after immersion in saturated $Ca(OH)_2$ solution (d), potentiometric response of Ag/AgCl electrode for different NaCl concentrations, after 2 days of immersion in saturated $Ca(OH)_2$ solution (e), and respective calibration curve (f).

E-t transient is presented in Fig. 3 a). As expected, the AgCl film growth began with the formation of rounded nuclei until the first layer was completed. In the initial growth stage, the ionic transport between the dissolving silver electrode and the electrolyte took place through the spaces between AgCl particles. As the film grew and the spaces between the first nuclei became covered, micro-channels (as shown in Fig. 3 b) were formed through AgCl to allow ionic transport.

The potentiometric response of the Ag/AgCl sensors was measured in saturated $Ca(OH)_2$ solution to mimic the mortar environment. A potential problem of Ag/AgCl electrodes embedded in cementitious materials is the dissolution and exfoliation of the AgCl film due to the contact with hydroxide ions for long periods [35], which decreases the available interfacial area for the electrochemical equilibrium leading to the failure of the sensors. So, the test was extended for 74 days to confirm the maintenance of the potentiometric response in these high pH conditions over time. The calibration curves and the variation of slope (m) with time of immersion are presented in Fig. 3 c) and 3 d), respectively. After a small shift in the first day of immersion, the calibration curves presented a quasi-Nernstian response, practically identical from the first to the last day of the test. Consequently, all the Ag/AgCl electrodes were characterized after 2 days of immersion in the simulated pore solution for different NaCl concentrations. Fig. 3 e) and 3 f) show typical results. The sensor response was almost immediate (few seconds) and stable over time. The calibration curve presented a limit of detection near 10^{-5} M and a sub-Nernstian slope of 53.2 mV pH^{-1}. This is possibly related to the limited ionic transport until the interfacial region between silver and silver chloride due to the film thickness and the small size of the micro-channels.

3.2. Chloride ingress in mortars

The chloride concentration inside the reference mortar (without LDH) and in a mortar with 2 wt% LDH-NO_2 is presented in Fig. 4. The recorded potential values were converted to chloride concentration via previously obtained calibration curves. The first observation from the results is the faster ingress of chloride ions in the reference mortar. The mortar with LDH was able to delay the ingress of chloride ions. After 20 days of immersion, only the sensor at 5 mm detected chloride, while in the reference mortar, chloride was already being detected at a depth of 20 mm.

Explanations that have been advanced for the slower progression of chloride ions in samples with LDH include the decrease of porosity induced by the presence of LDH particles [36] and the Cl^- capture by the LDH via an ionic exchange mechanism [10]. The same ZnAl-NO_2 LDH has been investigated before and showed a preference for capturing OH^- over Cl^- and, furthermore, it partially dissolved at high pH [6,37]. This makes the above mechanisms unlikely to occur. Since the chloride ingress was slower in the mortar with LDH, an alternative mechanism to Cl^- entrapment must be operating. It was postulated that the LDH dissolution could release aluminium ions which would react with the chloride ions from the pore solution, forming a new chemical compound, removing the chloride ions from solution and sequestering them in the cementitious phase [6,37].

3.3. Analysis of mortar

In parallel with the chloride sensing, mortar samples were removed from solution after 0, 6, 16 and 65 days of immersion. The cores were extracted through dry cut, sliced into 5 mm sections, ground, and mixed with distilled water. The chloride content present in each solution was measured potentiometrically with a commercial chloride ion-selective electrode. Fig. 5 presents the evolution of chloride content per kg of mortar, as a function of depth, of samples with and without LDH-NO_2.

After 65 days of immersion, the samples with LDH-NO_2 presented 3.8, 2.7 and 0.7 g of chloride per kg of mortar, at depths of 2.5, 7.5 and 12.5 mm, respectively. The reference samples only contained 2.1, 1.4 and 0.4 g of chloride per kg of mortar, for the same depths. The sample with LDH presented higher chloride content compared to the reference mortar. These results indicate that the removal of chloride ions from solution leads to an increase in the bound chloride content, which in turn will lead to an increase in the total amount of chloride (free and bound chloride). The capture of chlorides from the pore solution maintains the concentration gradient between pore solution and external electrolyte constant and, consequently, promotes the entry of a greater amount of chlorides. Interestingly, the samples with and without LDH-NO_2 have a similar maximum penetration depth — about 15 mm — after

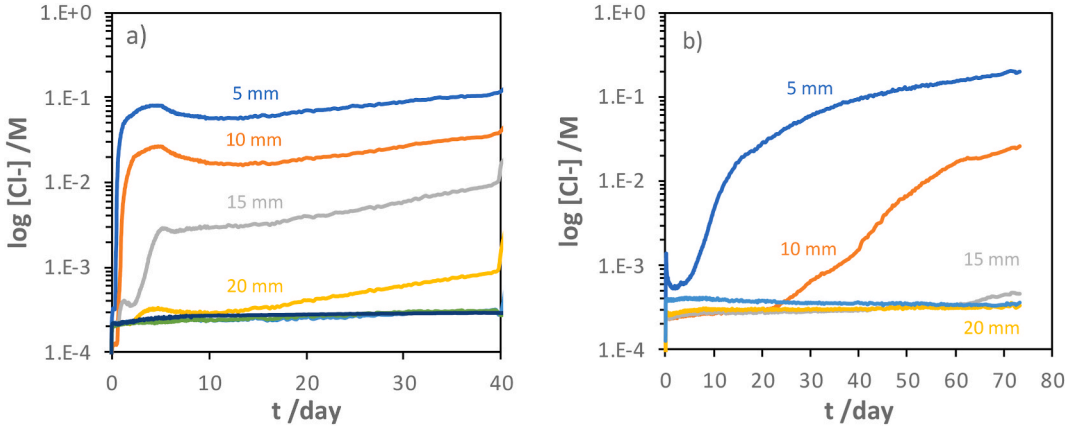

Fig. 4. Potentiometric response of embedded Ag/AgCl sensors, at different depths (5, 10, 15, 20, 25, 30 and 35 mmm), in mortar samples without (a) and with LDH (b) immersed in 3.5 % NaCl.

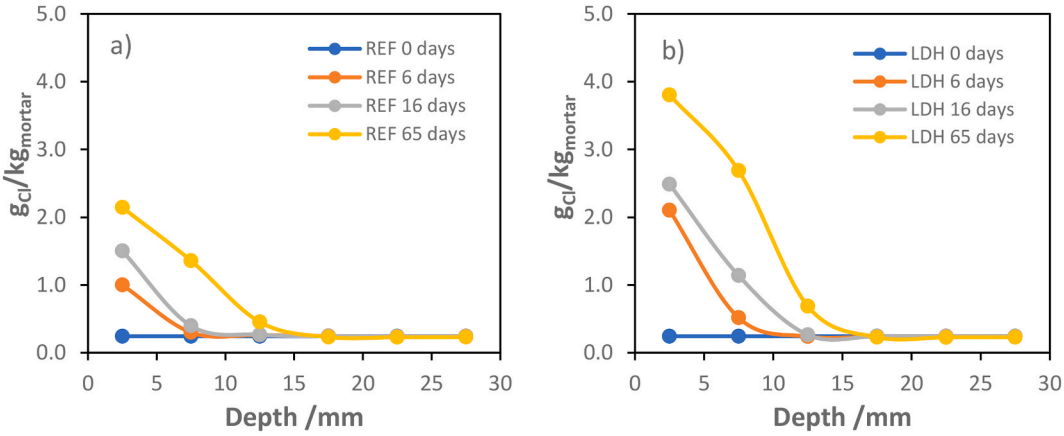

Fig. 5. Depth profile evolution of chloride content in mortar samples without (a) and with LDH (b), for 65 days of immersion, obtained by destructive analysis.

65 days of immersion, which suggests a similar progression of electrolyte through the pore network in both samples.

The indirect capture of chlorides through the formation of Friedel's salts is a process described in the literature [38]. As such, it was necessary to analyze the different phases present in the mortar samples after immersion in the chloride solution to understand the possible influence of the formation of these salts on the slower evolution of the chloride concentration. The mortar powders were analyzed by XRD to identify the different phases present. Fig. 6 a) and 6 b) show, respectively, the diffractograms of the mortar samples without and with LDH-NO_2 taken at different days of immersion (0, 6, 16 and 65 days) from the layer close to the NaCl solution (0–5

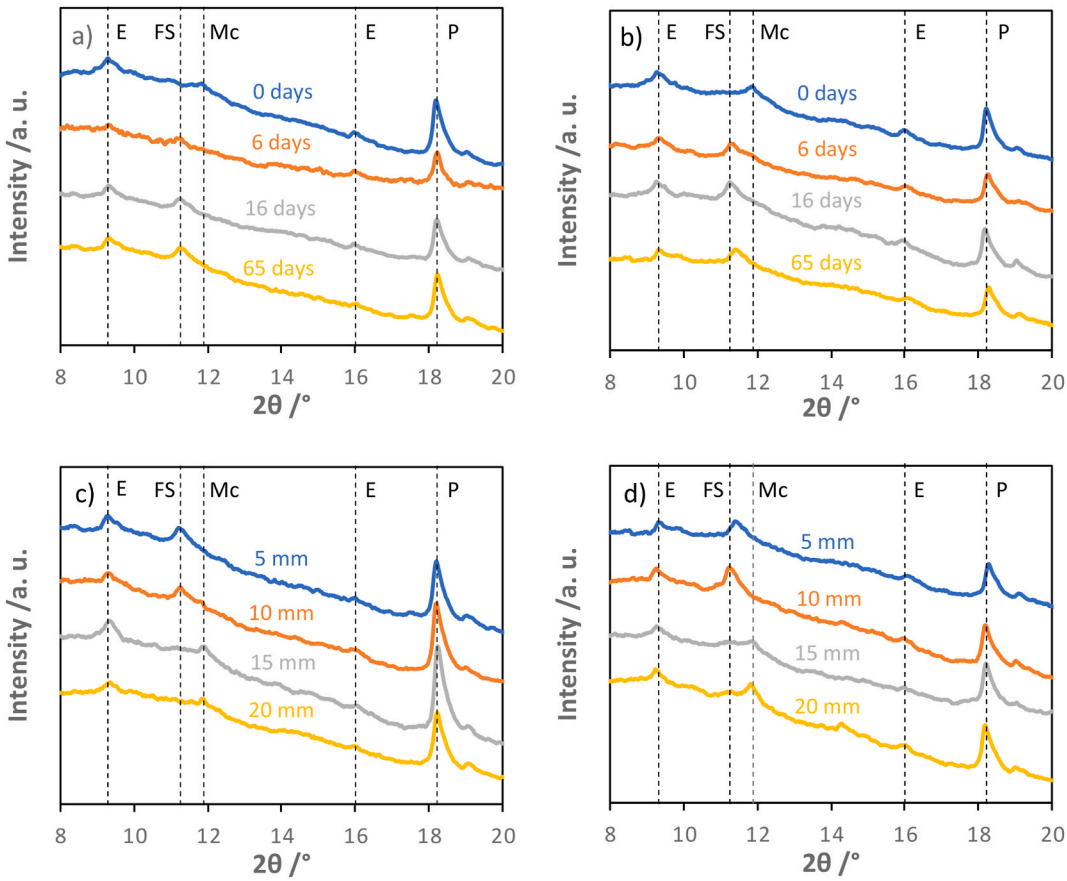

Fig. 6. Diffractograms of ground mortar samples without (a) and with (b) LDH-NO_2, at 0–5 mm of depth, for different time of immersion (0,6, 16 and 65 days), and diffractograms of reference (c) and with LDH (d) samples after 65 days of immersion, for different depths (0–5, 5–10, 10–15 and 15–20 mm). The identified phases were ettringite (E), Friedel's salts (FS), portlandite (P), and monocarbonate (Mc).

mm of depth). Fig. 6 c) and 6 d) show, respectively, the diffraction patterns of mortar without and with LDH, after 65 days of immersion, at different depths (0–5, 5–10, 10–15 and 15–20 mm). The diffractograms depict the reflections of ettringite (E, $Ca_6Al_2(SO_4)_3(OH)_{12}{\cdot}26H_2O$) at 9.3° and 16°, Friedel's salt (FS, $Ca_4Al_2(OH)_{12}Cl_2.4H_2O$) at 11.25°, monocarbonate (or monocarboaluminate, Mc, $Ca_4Al_2(CO_3)(OH)_{12}{\cdot}5H_2O$) at 11.9°, and portlandite (P, $Ca(OH)_2$) at 18.22° [39,40]. At the beginning of immersion (t = 0) the phases E, Mc and P are present but not FS. With time, as the chloride ions enter the mortar, Mc is replaced by FS. The monocarboaluminate reacts with chloride ions and forms Friedel's salt [41].

In another set of experiments, ground material from regions at depths of 0–5 mm and 5–10 mm of mortars immersed in 3.5 % NaCl for 65 days were analyzed by TGA. The results are presented in Fig. 7 a) and b). The corresponding differential plots (DTG) are presented in Fig. 7 c) and d). Three major weight losses were observed, one at 80–90 °C attributed to ettringite (E), another at 420–430 °C assigned to portlandite (P), and a third at 660–680 °C due to calcium carbonate (CC) [41]. A small weight loss at 280–380 °C was attributed to Friedel's salt (FS) – see inset of Fig. 7 c) – due to the decomposition of the FS main layer water. The quantity of FS was estimated according to Ref. [41]:

$$m_{FS} = \frac{M_{FS}}{6M_W} m_W \tag{3}$$

where m_{FS} is the mass ratio of FS in the mortar, M_{FS} is the molar mass of FS (561.3 g mol^{-1}), m_W is the integrated area of the FS weight loss peak (inset of Fig. 7 c), and M_W is the water molar mass (18.02 g mol^{-1}). The quantity of FS at the 0–5 mm level on the mortars with LDH was 0.34 wt% and 0.30 wt% on the mortar without LDH. The higher amount of FS on the mortar with LDH can be explained by the additional contribution of the partial LDH dissolution to the formation of FS. However, the difference between mortars is too small to explain the much higher capture of chlorides by the mortar with LDH compared to the reference mortar. The low contribution of Friedel's salt formation to the measured total chloride content was observed before [26]. These results corroborate the positive effect of LDH. The capture of chlorides is possibly due to ionic exchange or surface adsorption with the undissolved ZnAl-NO_2 LDH.

3.4. Corrosion of iron wires

Experiments were performed with iron electrodes embedded in the mortar samples to simulate the steel reinforcement. Three types

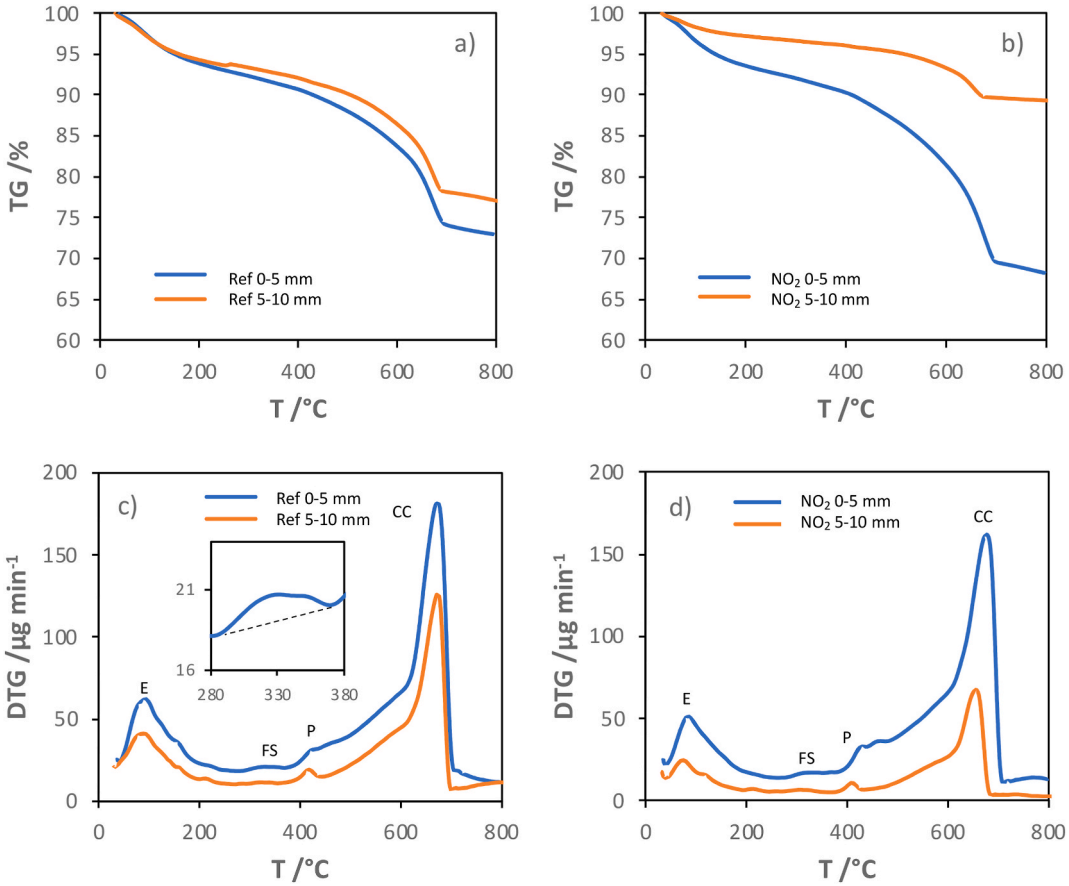

Fig. 7. TG and DTG curves of ground mortar samples without (a and c) and with LDH-NO_2 (b and d), exposed to chlorides for 65 days, for different depths (0–5 and 5–10 mm). The identified phases were ettringite (E), Friedel's salts (FS), portlandite (P), and calcium carbonate (CC).

of mortar were tested: mortar without LDH (reference), mortar with LDH-NO_3 (with the ability to bind chloride ions), and mortar with LDH-NO_2 (chloride binding ability plus the release of corrosion inhibiting nitrite ions). The evolution of the open circuit potential (corrosion potential) of the iron electrodes with the immersion time is shown in Fig. 8. The results of the electrodes at 5 mm were discarded due to the large heterogeneity of the outer surface which led to very scattered data. The OCP of all others was initially around −0.1 V *vs*. SCE, which is typical of passive steel inside mortar [1,[42]]. Then, the potential of the electrodes at 10 and 15 mm in the reference mortar dropped until reaching the values of the active corrosion of iron (close to −0.6 V_{SCE}) after, respectively, 5 and 10 days. The potential of the iron electrodes in the LDH-containing mortars remained in the passive region through the 30 days testing period. These results agree with the chloride distribution found in section 3.2., which showed that during the first month of immersion chloride progressed 15 mm in the reference sample, but only 5 mm in the sample with LDH-NO_2. The high OCP in the two systems with LDH is indicative of lower chloride content in the pore solution and a proof of the positive effect of the LDH addition.

The electrochemical state of the iron wires was also accessed by EIS. Fig. 9 presents Bode diagrams of the impedance of the iron electrodes at 10, 15, 20 and 25 mm measured on the 28th day of immersion. In the reference mortar, the wires at 10 and 15 mm showed very low impedance indicating an advanced state of corrosion. The electrodes at greater depth seemed to be still in a passive state, but already showing a resistive response at lower frequencies.

The time constant (relaxation process) centered around 1–10 Hz can be related to a surface film (either a passive film or a layer of corrosion products) and the time constant at lower frequencies can be ascribed to the corrosion process, with the double layer capacitance, C_{DL}, and the charge transfer resistance, R_{CT}. In the case of mortars with LDH, after 1 month of immersion, the electrodes presented high impedance, with just slight differences in depth. The response of the wires in the mortar with LDH-NO_3 was dominated by a single time constant while the impedance in mortars with LDH-NO_2 showed two time constants.

To help assigning the time constants to the proper physico-chemical processes, the impedance spectra were numerically fitted. For this purpose, the ZView program (Scribner Associates, USA) was used considering the equivalent electric circuit shown in Fig. 10, where R_{HF} is the resistance at high frequency, related to the resistance of the solution in the pores of the mortar, R_{PL} and C_{PL} are, respectively, the resistance and capacitance of the passive film formed on the iron surface, and C_{DL} and R_{CT} are the parameters associated with the corrosion at the metal surface, already identified above.

This circuit omits the solution resistance, i.e., the resistance of the solution between the reference electrode and the mortar surface

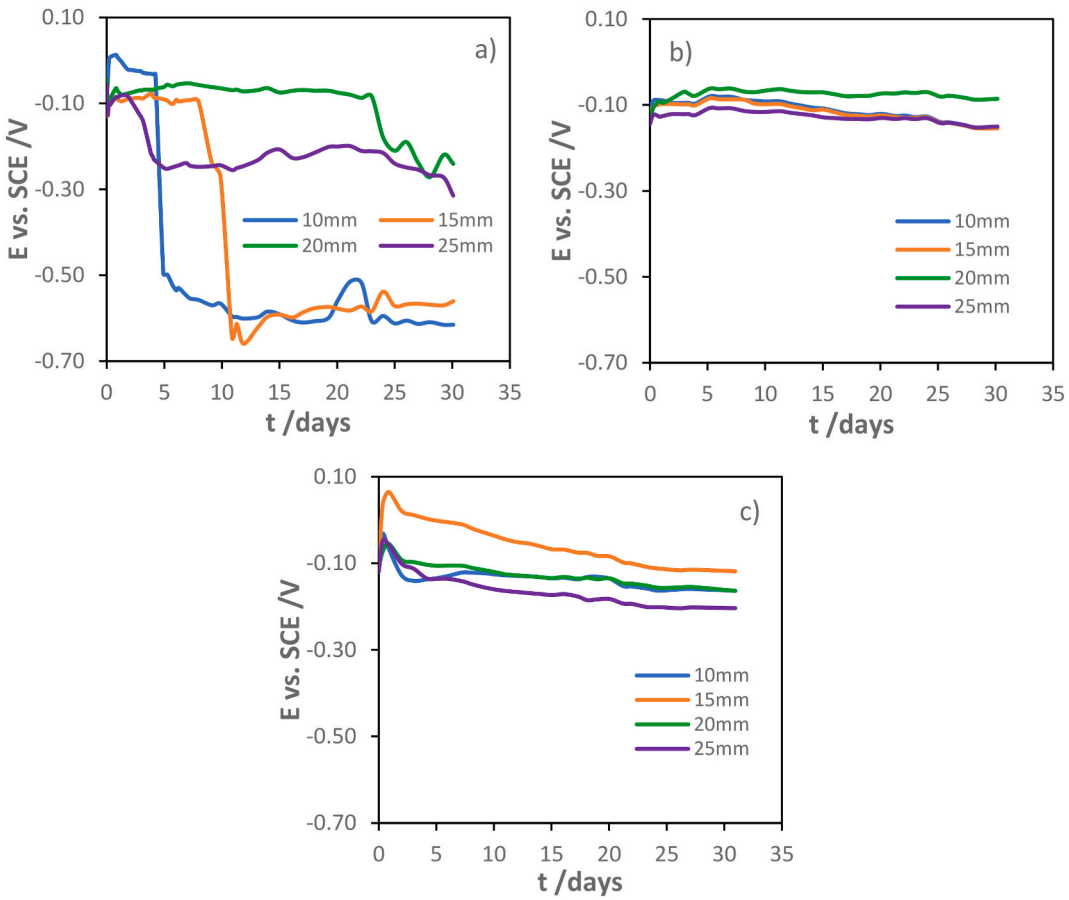

Fig. 8. OCP evolution of iron electrodes embedded in mortar samples without additive (a), with LDH-NO_2 (b) and with LDH-NO_3 (c), at different depths (10, 15, 20 and 25 mm), for 30 days of immersion in 3.5 % NaCl solution.

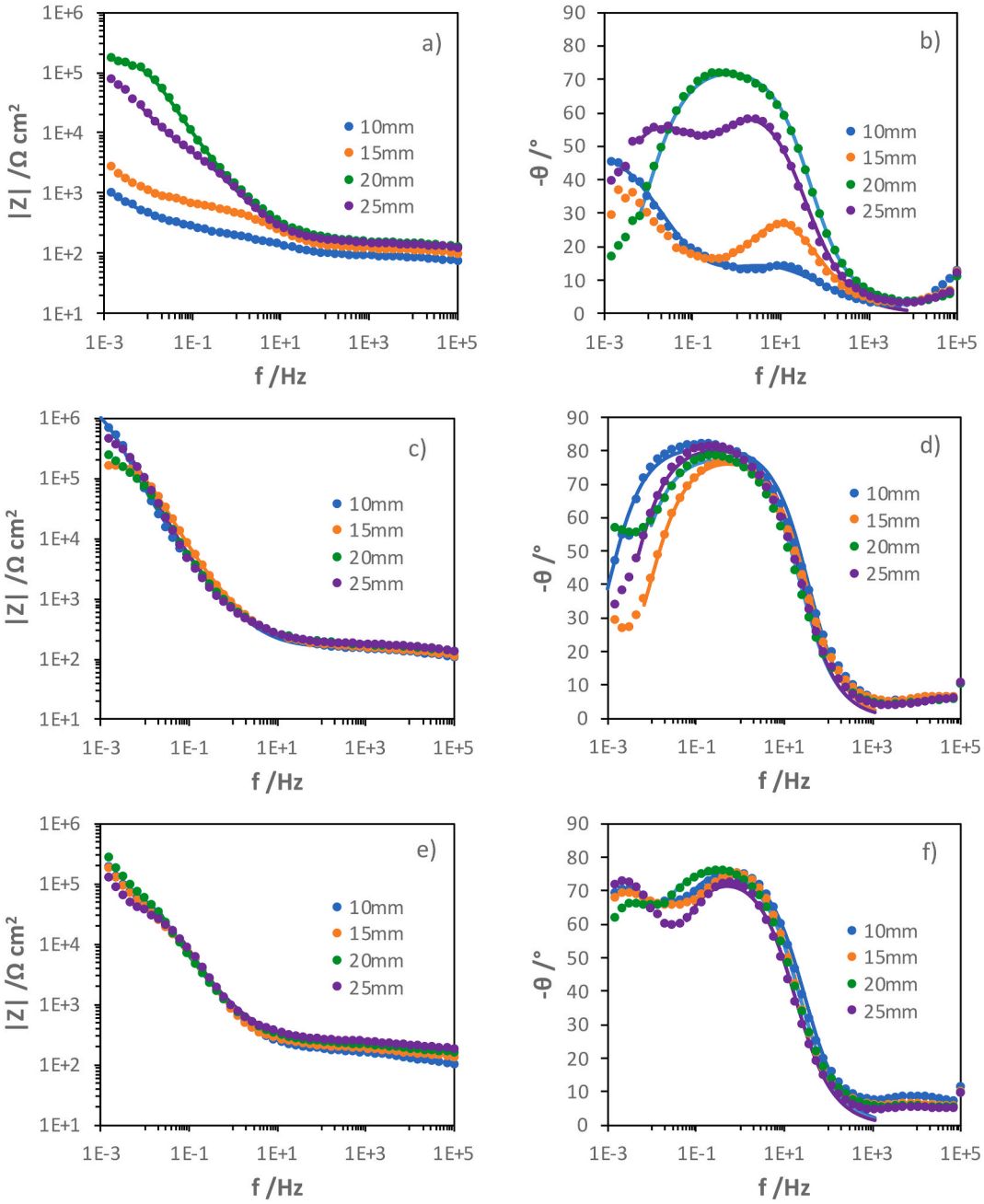

Fig. 9. Bode diagrams of iron electrodes embedded at different depths (10, 15, 20 and 25 mm) in mortars without LDH (a and b), with LDH-NO_3 (c and d) and LDH-NO_2 (e and f), at different distances from the surface (10, 15, 20 and 25 mm) after 28 days of immersion.

because it was not measured (higher frequencies would be needed). The capacitance of the mortar layer (C_{HF}) is also not included in the circuit because it is only detected in some spectra and even then, with poor definition. As a result, the fittings were performed in the region of the spectra below 1 kHz. In addition, owing to their non-ideal behaviour, the capacitances were replaced by constant phase elements (CPE) in the fitting procedure [43]. The impedance of a CPE is given by,

$$Z_{CPE} = \frac{1}{Y_0\ (j\ \omega)^n} \tag{4}$$

where Y_0 is the frequency independent admittance, n is the power of the CPE, $j = \sqrt{-1}$ and ω is the angular frequency (in radians). After the fitting, the CPE values were converted to capacitances using the Brug equation [44],

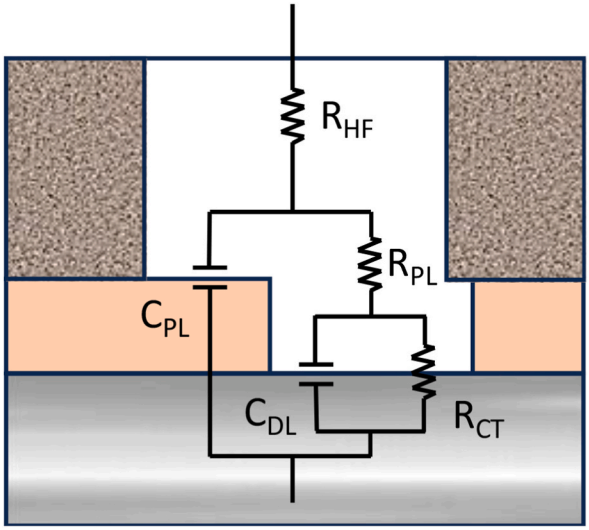

Fig. 10. Equivalent electrical circuit used to fit the impedance spectra.

$$C = \sqrt[n]{Y_0}\left(\frac{1}{R_1}+\frac{1}{R_2}\right)^{\frac{n-1}{n}} \tag{5}$$

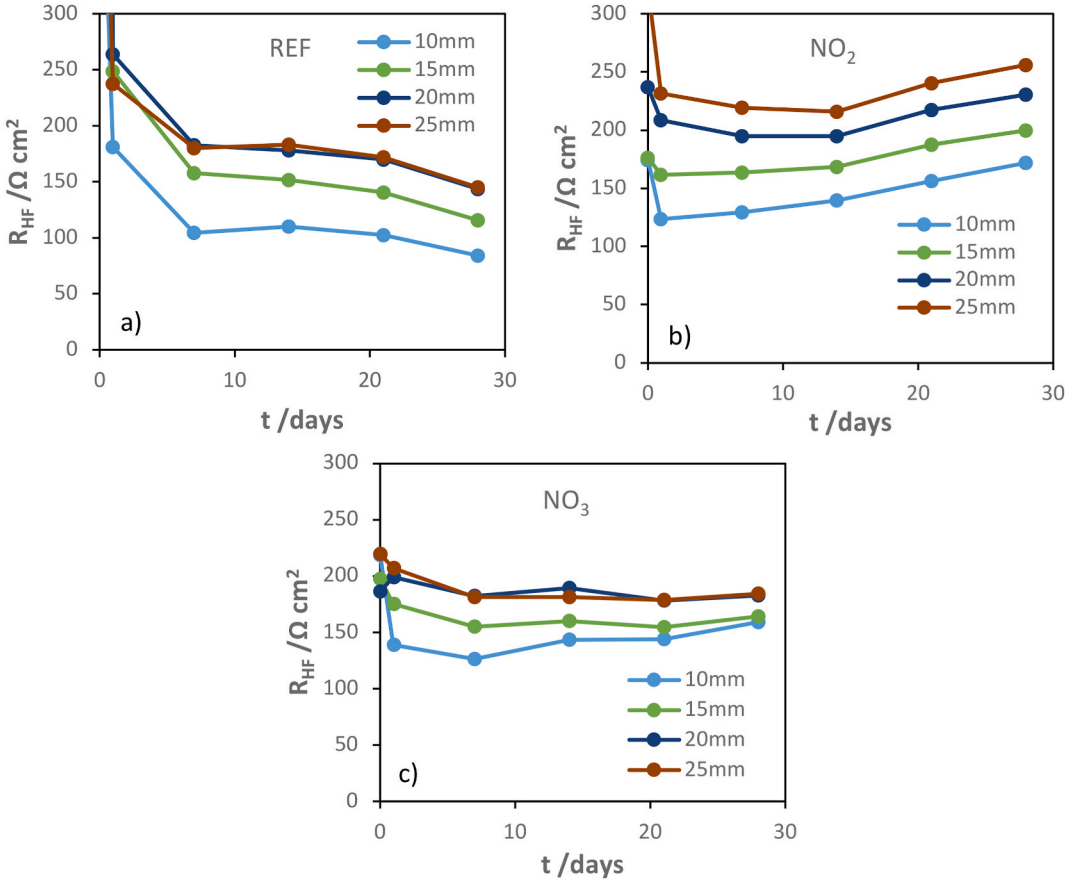

Fig. 11. Evolution of the resistance at high frequencies of mortar samples at different depths (10, 15, 20 and 25 mm) without additive (a), with LDH-NO_2 (b), and with LDH-NO_3 (c).

where R_1 and R_2 are the resistances in series and in parallel with the CPE, respectively.

While Fig. 9 shows the impedance after 28 days of immersion in 3.5 % NaCl, Figs. 11–13 present the evolution of the impedance parameters during the total immersion period. Fig. 11 exhibits the evolution of the resistance at high frequencies (R_{HF}) as a function of immersion time, at different distances from the surface (10, 15, 20 and 25 mm), for the three mortar samples. R_{HF} corresponds to the resistance of the solution inside the complex pore network of mortar [45]. It is influenced by the entrance of electrolyte ions (Cl^- and Na^+) and pore clogging. A considerable decrease in R_{HF} was observed in the first hours of immersion due to the ingress of solution into the pore network. It continued decreasing in the reference sample, as the chloride ions diffused through the pore network. In the samples with LDH, R_{HF} gradually increased after the 7th day of immersion, which can be explained by chloride ions entrapment and the continuing curing of the immersed mortar, leading to a decrease in the pores size and clogging. This is a sign of the action of LDH inside the mortar. R_{HF} is higher for the electrodes at greater depth due to the longer path from the solution to the electrode surface.

The other parameters of the reference sample are presented in Fig. 12. C_{OX} and R_{OX} appear instead of C_{PL} and R_{PL} to denote the existence of a layer of corrosion products (oxide layer) and not a passive film. This applies at least for the electrodes at 10 and 15 mm. C_{DL} and R_{CT} are related to the corrosion of the metal surface. R_{CT} increases with depth and decreases with time. The lower R_{CT} of the Fe wires close to the surface reflects their higher corrosion rate. This is a consequence of the local higher chloride content which destroys the passive film. In the cases where R_{CT} is low the corresponding C_{DL} has values much higher than that of a typical double layer (20–50 μF cm^{-2}). The high capacitance values are attributed to the formation of porous and conductive corrosion products which increase the electroactive surface area and to the adsorption of chemical species at that surface [46]. Alternatively, the impedance of this region of the spectrum for the wires with higher corrosion rate (low R_{CT}), like the ones at 10 and 15 mm in Fig. 9 a) and b), can be explained by a diffusional control of the corrosion process.

The impedance parameters of the samples with LDH are presented in Fig. 13. The impedance values of the wires in the mortar with LDH-NO_3 do not vary significantly, which means that the iron electrodes are still in a passive state in all places of the sample, with C_{PL} values around 30 μF cm^{-2} and R_{PL} values between 10^5 and 10^6 Ω cm^2. Given that the capacitance values are more typical of a double layer, it is possible to alternatively consider the capacitance to be C_{DL} and in such case the resistance in parallel would be R_{CT}. In either case the high impedance at low frequencies suggests a high corrosion resistance. This can be explained by the high pH of the pore solution and the lower chloride content due to the LDH.

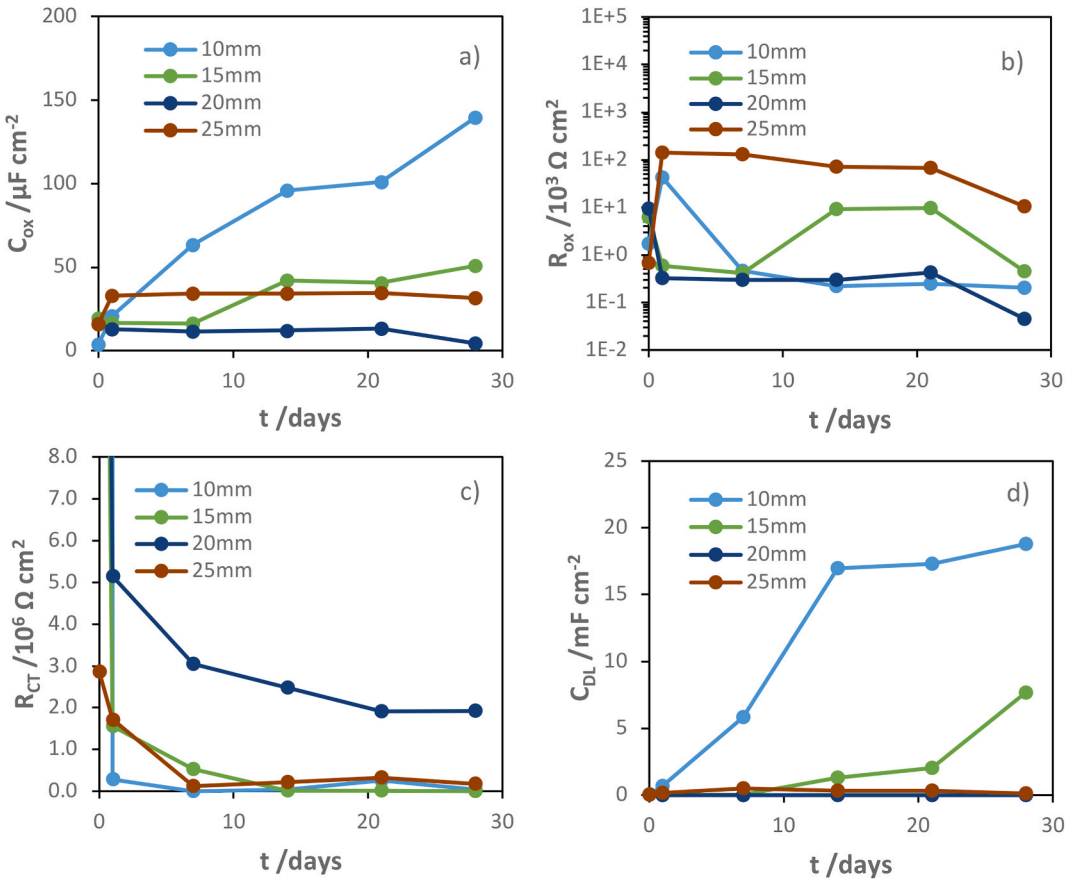

Fig. 12. Evolution of EIS parameters of the iron electrodes at different depths (10, 15, 20, and 25 mm) in the reference mortar: capacitance of a surface oxide layer (a), resistance of the surface oxide layer (b), double layer capacitance (c) and charge transfer resistance (d).

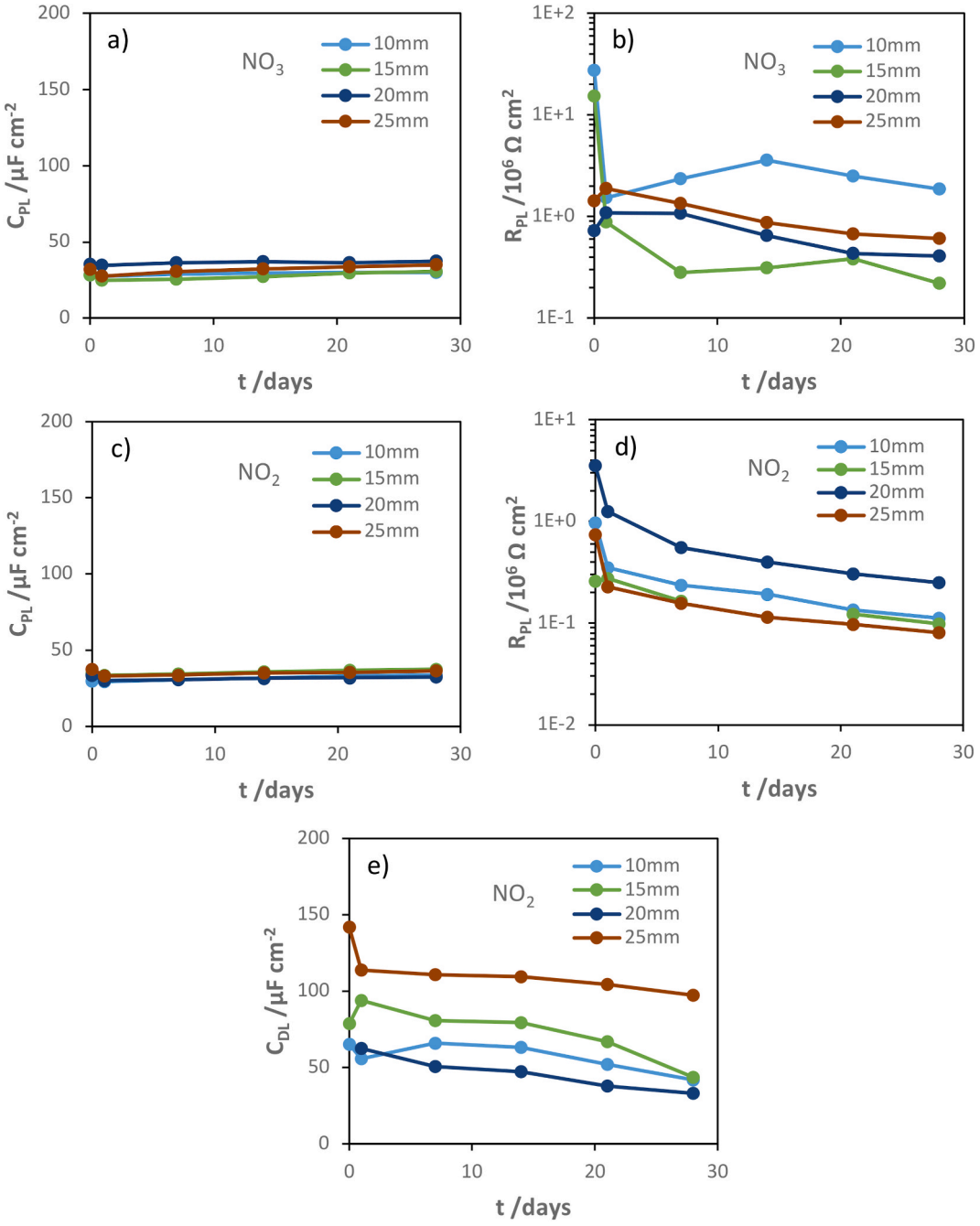

Fig. 13. Evolution of EIS parameters of iron electrodes at different depths (10, 15, 20 and 25 mm) in mortars containing LDH-NO_3 (a–b) and LDH-NO_2. (c–e). R_{PL} and C_{PL} are the resistance and capacitance of passive layer, respectively, and C_{DL} is the capacitance of double layer.

The impedance of the wires in the mortar with LDH-NO_2 presents 2 time constants, one at middle frequencies attributed to the response of the surface film (C_{PF} and R_{PF}) and the one at lower frequencies assigned to the corrosion (C_{DL} and R_{CT}). R_{CT} was so high that it was not actually measured in the tested frequency range.

Nitrite is an anodic inhibitor that reacts with the ferrous ions and forms a film of ferric oxide, Fe_2O_3 [46–49], according to,

$$2Fe^{2+}\,(aq) + 2OH^{-}\,(aq) + 2NO_2^{-}\,(aq) \rightarrow 2NO\,(g) + Fe_2O_3\,(s) + H_2O\,(l) \quad (6)$$

In the presence of chloride ions another iron oxide form is more stable, γ-FeOOH, and the reaction can be written as [48,49],

$$Fe^{2+}\,(aq) + OH^{-}\,(aq) + NO_2^{-}\,(aq) \rightarrow NO\,(g) + \gamma\text{-}FeOOH\,(s) \quad (7)$$

In any case a protective film is formed that passivates the iron surface, significantly lowering its corrosion rate. A drawback of the use of anodic inhibitors is the necessity of a minimum quantity to achieve full corrosion protection. An insufficient quantity leads to localised corrosion (e.g. pitting) which can be severe in the presence of aggressive species like chloride ions. For nitrite many studies report a critical molar concentration ratio $[NO_2^-]/[Cl^-]$ of 0.6 to guarantee corrosion protection (even though the interval spans from 0.5 to 1.5) [46,50]. The amount of LDH used in this work (2 % of total mortar mass) did not provide enough nitrite ions for a full protection and the impedance data displays the response of both the passive film and the localised corrosion.

3.5. Discussion

Initially, the effect of LDHs was tested by measuring the concentration of chlorides in the pore solution at different distances from the surface of mortar samples with and without LDH. On day 30th, the concentration of chlorides in the reference sample at distances of 5, 10, 15 and 20 mm was 83.82, 26.26, 5.95, and 0.61 mM, respectively, whereas in the sample with LDH, at the same distances, the concentration was 60, 0.6, 0.3 and 0.3 mM. The lower amount of chloride ions in the pore solution of the sample with LDH may be due to a structural variation of the cementitious matrix, namely an increase in its tortuosity [11] or a decrease in its porosity, and to the capture of chlorides, which can occur through the formation of Friedel salts or by anion exchange with LDHs. In order to validate the influence of LDHs on chloride entrapment, the evolution of the total amount of chlorides (bound and in the pore solution) was also studied, with a commercial sensor, in samples with and without LDH, and subjected to different immersion times. The analysis of the ground samples showed a greater content of chlorides in the sample with LDH. The reference sample after immersion for 65 days showed 2.14 and 1.36 g of chlorides per kg of mortar from 0 to 5 mm and 5–10 mm deep, respectively, while the sample with LDH, with the same immersion time, showed 3.80 and 2.69 g of chlorides per kg of mortar, at the same depths. This result refutes the hypothesis of a structural improvement, because it would lead to a decrease in the total amount of chlorides, contrary to what was obtained. In fact, an increase in the amount of LDH in mortar samples can lead to an increase in its porosity [13] and to higher chloride binding capacity in mortar. However, if the amount of LDH is lower than 2 vol%, the effect of LDH on mortar porosity is minimized [11].

Furthermore, the same samples used for the determination of total chloride content were analyzed by XRD and TGA to determine the hypothetical effect of chloride capture through the formation of Friedel salts (FS). FS ($Ca_2Al(OH)_6Cl.2H_2O$) are formed by the free chlorides binding with AFm (Aluminate Ferrite mono) hydrates [38,40,51,52]. The presence of FS was detected in both samples with and without LDH. However, the content of FS estimated from the TGA analysis was very similar for both samples (0.34 wt% and 0.30 wt% in the mortar with and without LDH, respectively, at 5–10 mm). The small increase of FS in the mortar sample with LDH can be explained by the contribution of chemical fixation of chlorides by LDH [36]. This result refutes the hypothesis that the capture of chlorides through the formation of FS is the phenomenon responsible for the lower concentration of chlorides in the pore solution of the mortar sample with LDH, measured by the sensors.

Finally, the effect of Zn-Al LDHs on corrosion protection of iron electrodes positioned at the same distances as the sensors was studied. At the beginning of the test, all electrodes presented an open circuit potential (-100 mV_{SCE}) characteristic of a passive state. After 10 days of immersion, the electrodes at 10 and 15 mm depth in the sample without LDH already showed signs of active corrosion, presenting an OCP close to −600 mV_{SCE}. In the case of the electrodes embedded in the mortar sample with LDH, they remained in a passive state even after 30 days of immersion. Impedance analysis showed that the presence of LDHs maintained the electrodes with a high charge transfer resistance (between 10^5 and 10^6 Ω cm^2). Furthermore, the evolution of solution resistance at different depths in samples with and without LDH was very similar, which shows that the presence of this additive does not significantly alter the microstructure of the mortar.

The effect of other LDHs, such as Mg-Al and Ca-Al LDHs on the corrosion protection of steel electrodes was studied by several authors [9,36,53,54]. The LDHs promoted an increase in the corrosion potential and charge transfer resistance of the electrodes in the presence of chlorides.

This work clearly demonstrates the positive effect of Zn-Al LDH on the capture of chloride ions in hardened mortar samples. The presence of LDH promoted a slower increase of chloride content in the pore solution of the samples, as shown by Ag/AgCl sensors, and maintained the iron reinforcements in a passive state, contrarily to the reference samples. The LDH loaded with nitrite protected the steel rebar from corrosion by the chloride capture and the inhibition effect. This is evident from the maintenance of a less negative corrosion potential and the presence of a time constant due to a surface film. However, the total chloride content was higher in the LDH-containing mortars, being most of it bound to the cementitious material. This poses a risk in the long run. In the case of structures subjected to carbon dioxide penetration, the consequent decrease in the pH of pore solution due to carbonation will lead to the release of the bound chlorides to the pore solution [55], and promote localized attack of the steel reinforcement. This is not a problem for submerged structures.

4. Conclusions

This work studied the effect of ZnAl-LDH on the chloride entrapment in mortar through in-situ monitoring of chloride concentration in the pore solution and chemical analysis of ground mortars. It also investigated the effect of ZnAl-LDH on the corrosion of embedded iron electrodes at different depths.

The mortars with LDH presented a much lower chloride concentration in the pore solution but a higher amount of chloride in the cementitious phase compared to the reference mortar. This is explained by the removal of chloride ions from the pore solution and its entrapment in the solid phase by the action of the ZnAl-LDH.

XRD and TGA analysis of ground mortars showed the presence of Friedel's salt in the mortars, with slightly higher amount in the mortars containing LDH. Higher corrosion was observed in the samples without LDH and at depths closer to the surface. The corrosion

at different depths is consistent with the distribution of chloride in the pore solution.

The capture of chlorides by LDH leads to an increase in the content of bound chlorides. The decrease in the pH of the pore solution over time, particularly due to the effect of carbonation, can lead to the dissolution of the solid phase and, consequently, increase the concentration of chlorides in the pore solution.

CRediT authorship contribution statement

R.S. Sampaio: Writing – review & editing, Writing – original draft, Validation, Methodology, Investigation, Conceptualization. **C. Gomes:** Investigation. **A.C. Bastos:** Writing – review & editing, Validation, Supervision, Conceptualization. **M.G.S. Ferreira:** Writing – review & editing, Supervision, Funding acquisition.

Declaration of competing interest

The authors declare that they have no known competing financial interests or personal relationships that could have appeared to influence the work reported in this paper.

Data availability

Data will be made available on request.

Acknowledgements

This work was funded by the HORIZON 2020 collaborative project "LORCENIS" (Long Lasting Reinforced Concrete for Energy Infrastructure under Severe Operating Conditions, Grant agreement nº 685445) and developed within the scope of the project CICECO-Aveiro Institute of Materials, UIDB/50011/2020, UIDP/50011/2020 & LA/P/0006/2020, financed by national funds through the FCT/MEC (PIDDAC). A.C. Bastos is funded by national funds (OE), through FCT - Fundação para a Ciência e a Tecnologia, I.P., in the scope of the framework contract foreseen in the numbers 4, 5 and 6 of the article 23, of the Decree-Law 57/2016, of August 29, changed by Law 57/2017, of July 19.

References

[1] P. Pedeferri, L. Bertolini, B. Elsener, E. Redaelli, R.B. Polder, Corrosion of Steel in Concrete - Prevention, Diagnosis, Repair, Wiley-VCH, 2013.
[2] K. Tuutti, Corrosion of Steel in Concrete (Doctoral Thesis, Monograph), Swedish Cement and Concrete Research Institute, Stockholm, 1982.
[3] M.R. Jones, D.E. Macphee, J.A. Chudek, G. Hunter, R. Lannegrand, R. Talero, S.N. Scrimgeour, Studies using 27Al MAS NMR of AFm and AFt phases and the formation of Friedel's salt, Cement Concr. Res. 33 (2003) 177–182, https://doi.org/10.1016/S0008-8846(02)00901-8.
[4] G.K. Glass, B. Reddy, N.R. Buenfeld, The participation of bound chloride in passive film breakdown on steel in concrete, Corrosion Sci. 42 (2000) 2013–2021, https://doi.org/10.1016/S0010-938X(00)00040-8.
[5] M. Chen, F. Wu, L. Yu, Y. Cai, H. Chen, M. Zhang, Chloride binding capacity of LDHs with various divalent cations and divalent to trivalent cation ratios in different solutions, CrystEngComm 21 (2019) 6790–6800, https://doi.org/10.1039/c9ce01322a.
[6] C. Gomes, Z. Mir, R. Sampaio, A. Bastos, J. Tedim, F. Maia, C. Rocha, M. Ferreira, Use of ZnAl-Layered double Hydroxide (LDH) to extend the service life of reinforced concrete, Materials 13 (2020) 1769–1788, https://doi.org/10.3390/MA13071769.
[7] Z.M. Mir, A. Bastos, D. Höche, M.L. Zheludkevich, Recent advances on the application of layered double hydroxides in concrete-A review, Materials 13 (2020) 1–23, https://doi.org/10.3390/ma13061426.
[8] S. Miyata, Anion-exchange Properties of Hydrotalcite-like Compounds, vol. 31, 1983, pp. 305–311.
[9] J. Xu, Q. Tan, Y. Mei, Corrosion protection of steel by Mg-Al layered double hydroxides in simulated concrete pore solution: effect of SO_4^{2-}, Corrosion Sci. 163 (2020), https://doi.org/10.1016/j.corsci.2019.108223.
[10] J. Xu, J. Wei, G. Ma, Q. Tan, Effect of MgAl-NO2 LDHs inhibitor on steel corrosion in chloride-free and contaminated simulated carbonated concrete pore solutions, Corrosion Sci. 176 (2020), https://doi.org/10.1016/j.corsci.2020.108940.
[11] Z.Y. Qu, Q.L. Yu, H.J.H. Brouwers, Relationship between the particle size and dosage of LDHs and concrete resistance against chloride ingress, Cement Concr. Res. 105 (2018) 81–90, https://doi.org/10.1016/j.cemconres.2018.01.005.
[12] P. Duan, W. Chen, J. Ma, Z. Shui, Influence of layered double hydroxides on microstructure and carbonation resistance of sulphoaluminate cement concrete, Construct. Build. Mater. 48 (2013) 601–609, https://doi.org/10.1016/j.conbuildmat.2013.07.049.
[13] Z. Yang, H. Fischer, R. Polder, Laboratory investigation of the influence of two types of modified hydrotalcites on chloride ingress into cement mortar, Cem. Concr. Compos. 58 (2015) 105–113, https://doi.org/10.1016/j.cemconcomp.2014.12.016.
[14] C.W. Chung, H.Y. Jung, J.H. Kwon, B.K. Jang, J.H. Kim, Use of calcium aluminum–layered double hydroxide to control chloride ion penetration of cement-based materials, J. Struct. Integr. Maint. 4 (2019) 37–42, https://doi.org/10.1080/24705314.2019.1565057.
[15] Z. Xu, Y. Wu, Z. Zhang, Y. Wang, J. Hu, Y. Ma, Z. Zhang, H. Huang, J. Wei, Q. Yu, C. Shi, A review on the research progress of LDHs as corrosion inhibitors for reinforced concrete, J. Build. Eng. 70 (2023) 106303, https://doi.org/10.1016/j.jobe.2023.106303.
[16] J. Tedim, A. Kuznetsova, A.N. Salak, F. Montemor, D. Snihirova, M. Pilz, M.L. Zheludkevich, M.G.S. Ferreira, Zn-Al layered double hydroxides as chloride nanotraps in active protective coatings, Corrosion Sci. 55 (2012) 1–4, https://doi.org/10.1016/j.corsci.2011.10.003.
[17] Y. Song, Y. Tang, L. Fang, F. Wu, X.G. Zeng, J. Hu, S.F. Zhang, B. Jiang, H.J. Luo, Enhancement of corrosion resistance of AZ31 Mg alloys by one-step in situ synthesis of ZnAl-LDH films intercalated with organic anions (ASP, La), J. Magnesium Alloys 9 (2021) 658–667, https://doi.org/10.1016/j.jma.2020.03.013.
[18] F. Wu, J. Liang, Z. Peng, B. Liu, Electrochemical deposition and characterization of Zn-Al layered double hydroxides (LDHs) films on magnesium alloy, Appl. Surf. Sci. 313 (2014) 834–840, https://doi.org/10.1016/j.apsusc.2014.06.083.
[19] Y. Abbas, F. Pargar, D.A. Koleva, K. van Breugel, W. Olthuis, A. van den Berg, Non-destructive measurement of chloride ions concentration in concrete – a comparative analysis of limitations and prospects, Construct. Build. Mater. 174 (2018) 376–387.
[20] M.S. Ribeiro, J. Lage, A. Gonçalves, Chloride assessment in structures. Influences of sampling and test location, Cement Concr. Res. 117 (2019) 82–90, https://doi.org/10.1016/j.cemconres.2019.01.002.
[21] R. Sampaio, A. Bastos, M. Ferreira, New sensors for monitoring pH and corrosion of embedded steel in mortars during sulfuric acid attack, Sensors 22 (2022) 5356–5369, https://doi.org/10.3390/s22145356.
[22] F. Schoefs, M. Torres-Luque, M. Sánchez-Silva, J.F. Osma, E. Bastidas-Arteaga, Non-destructive methods for measuring chloride ingress into concrete: state-of-the-art and future challenges, Construct. Build. Mater. 68 (2014) 68–81.

[23] C.P. Atkins, J.D. Scantlebury, P.J. Nedwell, S.P. Blatch, Monitoring chloride concentrations in hardened cement pastes using ion selective electrodes, Cem. Concr. Compos. 26 (1995) 319–324.
[24] A. Behnood, K. Van Tittelboom, N. De Belie, Methods for measuring pH in concrete: a review, Construct. Build. Mater. 105 (2016) 176–188.
[25] P. Sjöberg-Eerola, J. Bobacka, A. Lewenstam, A. Ivaska, All-solid-state chloride sensors based on electronically conducting, semiconducting and insulating polymer membranes, Sens. Actuators, B 127 (2007) 545–553.
[26] N.M. Kocherginsky, Z. Wang, Polyaniline membrane based potentiometric sensor for ascorbic acid, other redox active species and chloride, J. Electroanal. Chem. 611 (2007) 162–168.
[27] G.J. Janz, H. Taniguchi, The silver-silver halide electrodes: preparation, stability, reproducibility, and standard potentials in aqueous and non-aqueous media, Chem. Rev. 53 (1953) 397–437.
[28] M.F.L. Demele, R.C. Salvarezza, V.D.V. Moll, H.A. Videla, A.J. Arvia, Kinetics and mechanism of silver-chloride electroformation during the localized electrodissolution of silver in solutions containing sodium-chloride, J. Electrochem. Soc. 133 (1986) 746–752, https://doi.org/10.1149/1.2108667.
[29] R.G. Compton, G.H.W. Sanders, Electrode Potentials, Oxford Science Publications, 1996.
[30] G. Inzelt, A. Lewenstam, F. Scholz, Handbook of Reference Electrodes, Springer, 2013.
[31] H. Ha, J. Payer, The effect of silver chloride formation on the kinetics of silver dissolution in chloride solution, Electrochim. Acta 56 (2011) 2781–2791, https://doi.org/10.1016/j.electacta.2010.12.050.
[32] G.J. Janz, H. Taniguchi, The silver-silver halide electrodes: preparation, stability, and standard potentials in aqueous and non-aqueous media, Chem. Rev. 53 (1953) 397–437.
[33] P.J. Brewer, A.S. Leach, R.J.C. Brown, The role of the electrolyte in the fabrication of Ag|AgCl reference electrodes for pH measurement, Electrochim. Acta 161 (2015) 80–83.
[34] J. Tedim, S.K. Poznyak, A. Kuznetsova, D. Raps, T. Hack, M.L. Zheludkevich, M.G.S. Ferreira, Enhancement of active corrosion protection via combination of inhibitor-loaded nanocontainers, ACS Appl. Mater. Interfaces 2 (2010) 1528–1535, https://doi.org/10.1021/am100174t.
[35] Z. Zhang, J. Hu, Z. Xu, H. Huang, S. Yin, Y. Ma, J. Wei, Q. Yu, Degradation process of Ag/AgCl chloride-sensing electrode in cement extract with low chloride concentration, Corrosion Sci. 198 (2022) 110107, https://doi.org/10.1016/j.corsci.2022.110107.
[36] J. Zuo, B. Wu, B. Dong, F. Xing, J. Ma, G. Wei, Effects of nitrite ion intercalated CaAl and MgAl layered double hydroxides on the properties of concrete mortar, Cem. Concr. Compos. 145 (2024), https://doi.org/10.1016/j.cemconcomp.2023.105306.
[37] Z.M. Mir, C. Gomes, A.C. Bastos, R. Sampaio, F. Maia, The Stability and Chloride Entrapping Capacity of ZnAl-NO2 LDH in High Alkaline/Cementitious Environment, 2020, pp. 78–99.
[38] A.K. Suryavanshi, J.D. Scantlebury, S.B. Lyon, Mechanism of Friedel's salt formation in cements rich in tri-calcium aluminate, C. Camcte Res. 26 (1996) 717–727.
[39] G. Paul, E. Boccaleri, L. Buzzi, F. Canonico, D. Gastaldi, Friedel' s salt formation in sulfoaluminate cements: a combined XRD and Al MAS NMR study, Cement Concr. Res. 67 (2015) 93–102, https://doi.org/10.1016/j.cemconres.2014.08.004.
[40] T. Matschei, B. Lothenbach, F.P. Glasser, The AFm phase in Portland cement, Cement Concr. Res. 37 (2007) 118–130, https://doi.org/10.1016/j.cemconres.2006.10.010.
[41] Z. Shi, M.R. Geiker, B. Lothenbach, K. De Weerdt, S.F. Garzón, K. Enemark-Rasmussen, J. Skibsted, Friedel's salt profiles from thermogravimetric analysis and thermodynamic modelling of Portland cement-based mortars exposed to sodium chloride solution, Cem. Concr. Compos. 78 (2017) 73–83, https://doi.org/10.1016/j.cemconcomp.2017.01.002.
[42] H. Zheng, C.S. Poon, W. Li, Mechanistic study on initial passivation and surface chemistry of steel bars in nano-silica cement pastes, Cem. Concr. Compos. 112 (2020) 103661, https://doi.org/10.1016/j.cemconcomp.2020.103661.
[43] M.E. Orazem, B. Tribollet, Electrochemical Impedance Spectroscopy, second ed., Wiley, 2017.
[44] G.J. Brug, A.L.G. Van Den Eeden, M. Sluyters-Rehbach, J.H. Sluyters, The analysis of electrode impedances complicated by the presence of a constant phase element, J. Electroanal. Chem. 176 (1984) 275–295.
[45] M. Cabeza, P. Merino, A. Miranda, X.R. Nóvoa, I. Sanchez, Impedance spectroscopy study of hardened Portland cement paste, Cement Concr. Res. 32 (2002) 881–891, https://doi.org/10.1016/S0008-8846(02)00720-2.
[46] P. Gu, S. Elliot, R. Hristova, J.J. Beaudoin, R. Brousseau, B. Baldock, A study of corrosion inhibitor performance in chloride contaminated concrete by electrochemical impedance spectroscopy, ACI Mater. J. 94 (1997) 385–395.
[47] K. Soeda, T. Ichimura, Present state of corrosion inhibitors in Japan, Cem. Concr. Compos. 25 (2003) 117–122, https://doi.org/10.1016/S0958-9465(01)00058-0.
[48] J.M. Gaidis, Chemistry of corrosion inhibitors, Cem. Concr. Compos. 26 (2004) 181–189, https://doi.org/10.1016/S0958-9465(03)00037-4.
[49] T.A. Söylev, M.G. Richardson, Corrosion inhibitors for steel in concrete: state-of-the-art report, Construct. Build. Mater. 22 (2008) 609–622, https://doi.org/10.1016/j.conbuildmat.2006.10.013.
[50] B. Elsener, Corrosion Inhibitors for Steel in Concrete - State-Of-The-Art Report, EFC Series N°35, IOM Communications, Institute of Materials, London, 2001.
[51] U.A. Birnin-Yauri, F.O. Glasser, Friedel's salt, Ca2Al(OH)6(Cl,OH).2H2O: its solid solutions and their role in chloride binding, Cem. Concr. Compos. 28 (1998) 1713–1723.
[52] F.P. Glasser, A. Kindness, S.A. Stronach, Stability and solubility relationships in AFm phases. Part I. Chloride, sulfate and hydroxide, Cement Concr. Res. 29 (1999) 861–866, https://doi.org/10.1016/S0008-8846(99)00055-1.
[53] C. Jing, B. Dong, A. Raza, T. Zhang, Y. Zhang, Corrosion inhibition of layered double hydroxides for metal-based systems, Nano Mater. Sci. 3 (2021) 47–67, https://doi.org/10.1016/j.nanoms.2020.12.001.
[54] Y. Cao, S. Dong, D. Zheng, J. Wang, X. Zhang, R. Du, G. Song, C. Lin, Multifunctional inhibition based on layered double hydroxides to comprehensively control corrosion of carbon steel in concrete, Corrosion Sci. 126 (2017) 166–179, https://doi.org/10.1016/j.corsci.2017.06.026.
[55] G.K. Glass, N.R. Buenfeld, The presentation of the chloride threshold level for corrosion of steel in concrete, Corrosion Sci. 39 (1997) 1001–1013, https://doi.org/10.1016/S0010-938X(97)00009-7.